Materials and Design 90 (2016) 745–752

Contents lists available at ScienceDirect

Materials and Design

journal homepage: www.elsevier.com/locate/jmad

Micro porosity analysis in additive manufactured NiTi parts using micro computed tomography and electron microscopy

Saeed Khademzadeh [a,b], Simone Carmignato [c], Nader Parvin [a,*], Filippo Zanini [b,c], Paolo F. Bariani [b]

[a] Department of Mining and Metallurgical Engineering, Amirkabir University of Technology (Tehran Polytechnic), 158754413, Tehran, Iran
[b] Department of Industrial Engineering, University of Padova, 35131 Padova, Italy
[c] Department of Management and Engineering, University of Padova, 36100 Vicenza, Italy

ARTICLE INFO

Article history:
Received 1 September 2015
Received in revised form 26 October 2015
Accepted 31 October 2015
Available online 2 November 2015

Keywords:
Micro direct metal deposition
Inherent micro porosity
Controllable micro porosity
Micro computed tomography
Scanning electron microscopy
NiTi implants

ABSTRACT

Long-term fixation of biomedical implants is achievable by using porous materials. These kinds of materials can produce a stable bone-implant interface. A critical aspect in production of porous implants is the design of macro and micro pores. In this research, a micro direct metal deposition process, newly developed as a potential method for implant production, was used to fabricate porous NiTi parts. The effect of process parameters on formation and distribution of micro pores was analysed using micro computed tomography and scanning electron microscopy. The analysis showed that, by increasing the laser scanning speed, inherent micro porosity increases. Also, it was found that there is an optimum temperature to achieve minimum inherent micro porosity by micro direct metal deposition which is 300 °C for NiTi powder.

1. Introduction

Porous metallic implants are promising due to their inherent low elastic modulus which is close to the stiffness of real bone. Moreover, porous structure promotes osseointegration in fabricated implants [1]. Generally, orthopaedic porous scaffolds should mimic the morphology, properties and microstructure of real bone which includes micro (<20 μm) and macro (>100 μm) pores [2]. Different methods exist for porous materials fabrication. Some methods such as casting, vapour deposition and especially additive manufacturing, allow a greater control over pore size and distribution. By these methods, open-cell porous structures are possible to be fabricated. On the other hand, there are other methods such as decomposition of foaming agents in either molten or powder metal matrices, which allow lower control over the characteristics of pores. Using these methods result in close-cell porous structures [3]. Many works have been conducted on production of porous scaffolds with macro pores using additive manufacturing methods such as selective laser melting (SLM) [4,5] and laser engineered net shaping (LENS) [6,7]. In additive technologies, macro pores are possible to implement using computer-aided design (CAD). In addition, two different categories of micro pores can be obtained in laser melted parts. Melting process can cause the formation of the first category of micro pores. We use the term *inherent micro porosity* for the micro pores that are formed by melting process. This kind of porosity is non-controlled and substantial. Also, we use the term *controllable micro porosity* for pre-defined micro pores which can be manipulated by change in hatch distances or strategy of scanning as two main important process parameters in laser melting. Micro direct metal deposition (μDMD) is an additive manufacturing technique that produces parts with micro features from metal powders, using direct metal deposition (DMD) concept [8]. μDMD uses low energy laser beam to promote melting in an inert environment within a chamber. Orthopaedic implants with inherent and controllable micro porosities can be fabricated by μDMD due to the specific process parameters of this technique. Control over the architecture of micro pores is essential for porous scaffolds to serve as a bone implant [9,10]. An evolution from random distribution of micro pores to pre designed porosity based on specific process parameters is important to control the functional behaviour of porous scaffolds. Regular architecture of micro pores permits cells to be seeded in the core much more readily than random architecture scaffolds [11]. Porosity, spatial distribution and morphology of micro pores have impact on mechanical and biological properties of porous implants. Design of micro pores inside the materials for biomedical application is still under research. It is possible to control micro pore's percentage by adjusting of process parameters. Despite there is no direct control on inherent micro pore's shape, it is possible to indirectly control the predefined micro pore's shape by changing process parameters such

* Corresponding author.
E-mail addresses: khademzadeh@aut.ac.ir (S. Khademzadeh), simone.carmignato@unipd.it (S. Carmignato), nparvin@aut.ac.ir (N. Parvin), filippo.zanini@unipd.it (F. Zanini), paolo.bariani@unipd.it (P.F. Bariani).

http://dx.doi.org/10.1016/j.matdes.2015.10.161
0264-1275/

as hatch distance and scanning strategy as demonstrated in this research. In this paper, the effects of μDMD process parameters in obtaining fully dense NiTi were investigated. Moreover, the effects of μDMD process parameters on porosity, micro pore's shape and distribution were analysed.

2. Materials and methods

Mechanically alloyed nickel–titanium powder produced by MBN Nanomaterialia (Italy) with a Ni:Ti ratio of 50.8:49.2 (atomic %) was used in this research as a starting material. Characteristics of the powder are given in Table 1 and described in more details elsewhere [8]. MSL50 micro laser sintering machine (Manudirect Company, Italy) with a continuous fibre laser (YLM-100-WC, IPG, wavelength: 1070 nm), maximum power of 100 W and 30 μm minimum laser spot diameter was used to implement single tracks, thin walls and small cubes. A schematic representation of the system is shown in Fig. 1. Using a heating stage and Argon filled chamber, it is possible to increase and control the temperature of parts during the process. Fabrication of thin walls with different process parameters is the easiest way to investigate the effect of input energy on inherent micro pore's morphology and distribution in laser melted parts. To achieve the thickness of each layer produced by a single laser scan, a series of single tracks were processed using different scanning speeds (V), powder feeding rates (RF_n) and substrate temperatures (T) as shown in Table 2 and Fig. 2(a). The heights of single tracks were measured using a state-of-the-art 3D optical profiler (Sensofar Plu Neox, SENSOFAR-TECH, SL, Spain) operating in confocal mode [12] by calculating of arithmetic mean values of heights from horizontal sections on each single track (Fig. 2(b)).

288 thin walls were produced according to Table 3. The overlap was considered constant for all successive layers in each wall and was driven from Eq. (1).

$$\text{Overlap}\% = \frac{\text{Overlap length}}{\text{Layer thickness}} \times 100\% \quad (1)$$

Fig. 3 schematically shows the overlap between the successive layers. The heights of thin walls were measured by 3D optical profilometry, using the same procedure of single tracks.

Micro X-ray computed tomography (μCT) is a three-dimensional (3D) non-destructive imaging technique that allows the investigation of internal and external structures of parts and small features, with micrometric resolution [13,14]. In this research, μCT is used to analyse the porosity in 3D volume of laser melted parts. Such information can be used to improve the μDMD process; for example, to minimize porosity by varying μDMD parameters. μCT can also be used for quality control in laser melting process. The samples were scanned using a metrological μCT system (Nikon X-Tek MCT225, Nikon Metrology/X-Tek Systems Ltd., UK) with 225 kV micro-focus X-ray source, 3 μm focal spot resolution, flat panel detector with 2000 × 2000 pixels (16 bit), and temperature-controlled cabinet. The samples were placed on a rotating stage and a number of two-dimensional (2D) X-ray projections were acquired at various angular positions. Such projections were used to reconstruct a 3D model, by means of a filtered back-projection algorithm. The used CT scanning parameters are listed in Table 4. Distribution and volume of internal pores were analysed using commercial volume imaging software (VG Studio MAX, Volume Graphics GmbH, Germany). The porosity percentage related to the central part of each wall (shown in red in Fig. 4) was provided by calculating the total volume of pores against the total selected volume.

Table 1
Characteristics of initial powder.

	Nickel (%)	Titanium (%)	Particle size [μm]
NiTi powder	50.8	49.2	28–35

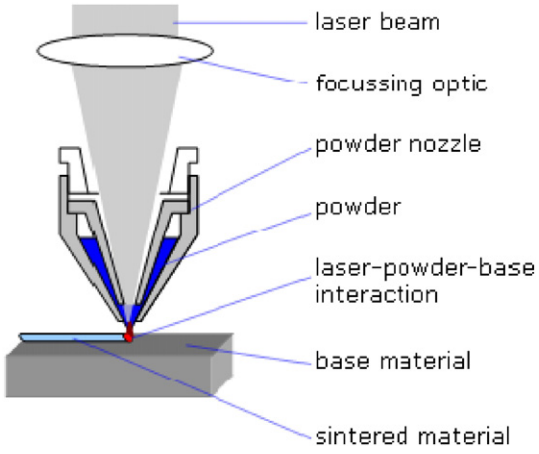

Fig. 1. Schematic representation of micro direct metal deposition system.

Controllable micro pores were implemented by varying μDMD process parameters. To analyse the effect of scanning strategy on controllable micro pore's morphology and distribution, different strategies based on the angles between tracks (θ_T) and layers (θ_L) were examined in this research to produce NiTi cubes. According to Table 5, five different strategies were employed to produce 5 NiTi cubes on titanium substrates (Fig. 5). Shape, sizes and distribution of micro pores in NiTi cubes were analysed using a scanning electron microscope (SEM) (Quanta 450, FEI). Porosity measurements were conducted on polished specimens, by performing image analysis of SEM micrographs. Also, the effect of hatch distance (d_H) on micro pore's morphology was investigated using this technique. To investigate the surface quality of laser melted NiTi cubes, roughness was measured using 3D optical profilometry.

3. Results and discussion

3.1. The effects of μDMD process parameters on geometry and inherent micro porosity of thin walls

In this chapter the effects of layer overlap, scanning speed and substrate temperature on the height of single tracks and thin walls are presented. Moreover, the effects of these parameters on quantity and distribution of inherent micro pores are described. Total input energy produced by μDMD can be calculated using Eq. (2). [15]:

$$E_L = \frac{P}{V \times \Delta Z \times d} \quad (2)$$

where P is power of laser, d is diameter of laser focus spot; V is the scanning speed and ΔZ is the pre-defined thickness of each layer. Increase in layer thickness and scanning speed as main μDMD process parameters results in decrease of input energy in laser melting according to Eq. (2). Low input energy causes discontinuous single tracks and inhibits the formation of 3D parts. On the other hand, at very high level of input energy, the temperature of melt pool

Table 2
μDMD process parameters used to produce NiTi single tracks.

Laser power (W)	Scan speed (mm/min)	Powder feeding rate (mg/min)	Substrate temperature (°C)	Internal energy density (kJ/mm^2)
30	70, 100, 150, 200	0.76, 1.26	200, 300, 400	0.3, 0.4, 0.6, 0.85

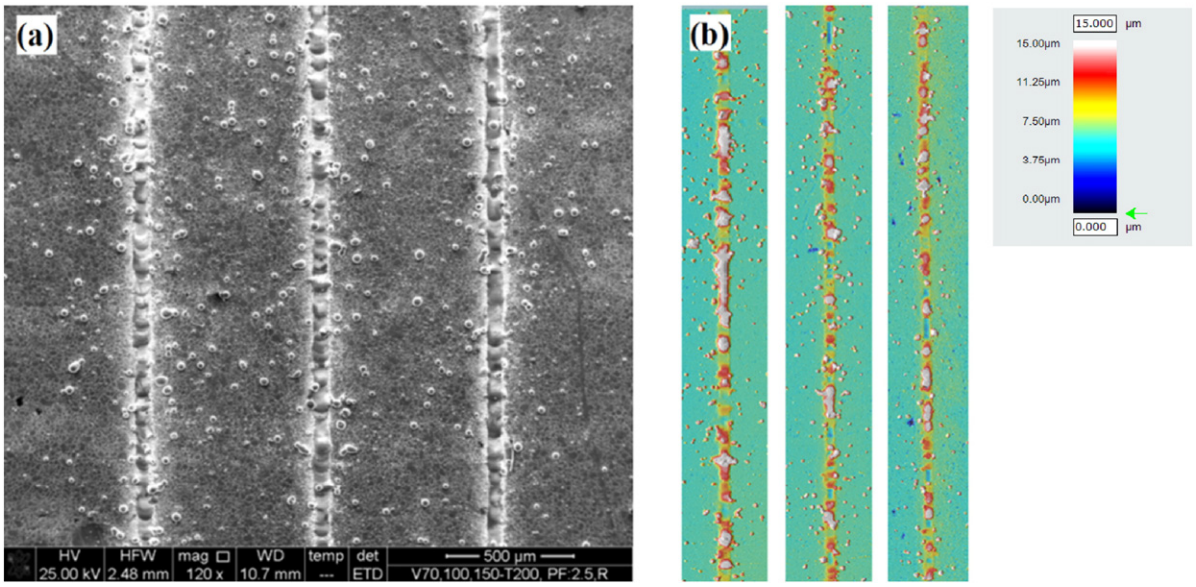

Fig. 2. (a): SEM image of NiTi single tracks produced by µDMD (RF_n: 1.26 mg/s), (b): 3D optical profiles of NiTi single tracks.

increases and evaporation of material may occur. High surface quality and high level of densification are obtainable by adjusting the scanning speed and thickness of layers. Moreover, other parameters such as powder feeding rate and substrate temperature can affect the formation of 3D parts by µDMD. Heating the substrate can accelerate the formation of melt pool even at low input energies. As it can be seen in Fig. 6(a), when the powder feeding rate isn't enough to form a continuous single track, heating of substrate hasn't significant effect on 3D part formation especially at high velocities. But, by increasing the feeding rate from 0.76 mg/s to 1.26 mg/s (Fig. 6(b)), the effect of substrate's temperature is more sensible. From Fig. 6(b), it can be easily understood that an increase in scanning speed reduces the height of single tracks. Moreover, high temperature of substrates facilitates the formation of 3D parts and increases the height of single tracks. In other words, high temperature can compensate the effect of high scanning speed and maintain the rate of growth.

Single track's height can be considered as nominal layer thickness which is possible to produce with specific µDMD process parameters. Nominal height (NH) of a thin wall which consists of successive single tracks can be simply calculated using Eq. (3):

$$NH = n \times H \tag{3}$$

Table 3
µDMD process parameters used to produce NiTi thin walls.

Laser power (W)	Scanning speed (mm/min)	Powder feeding rate (mg/min)	Substrate temperature (°C)	Number of layers	Overlap%
30	70, 100, 150, 200	0.76, 1.26	200, 300, 400	2, 5, 10, 30	0, 10, 30

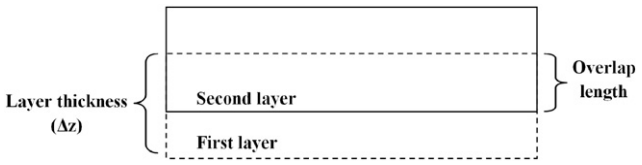

Fig. 3. Schematic of layer array and overlap between layers.

where NH is the nominal height of thin wall, *n* is the number of layers and *H* is the nominal thickness of single track. As can be seen in Figs. 7, 10% overlap between the layers in thin walls decreases the difference between the nominal height and the experimental height. It's notable to say that, the experimental heights are usually more than expected nominal heights driven from Eq. (3); this can be attributed to the temperature of substrate. In fact, accumulation of heat input, increases the temperature of melt pool and subsequently the rate of melting. Fig. 6(b) shows that by increase in substrate temperature, the height of single tracks and consequently the thickness of layers in thin walls increases. Geometry analysis using µCT scanning revealed that, by inserting the overlap between the layers in µDMD process, regular thin walls are obtainable (see Fig. 8(b,d)). The rate of growth at the beginning and the end of wall is more than in the central parts of the walls without interlayer overlap. This can be attributed to the layer thickness. As stated before, high pre-defined ΔZ for laser movement results in low input energy which inhibits 3D part formation (Fig. 8(a,c)). However, higher parts exist at the beginning and the end of thin walls because of more exposure time that occurs when the laser changes the direction of travelling between the layers. As it can be seen in Fig. 8(c,d) , by increasing the temperature of substrate from 200 °C to 300 °C, the heights of thin walls totally increase. Similar heat treatment was proposed by Shishkovsky et al. [16] to obtain dense and crack-free NiTi parts by laser melting. Twelve different thin walls were selected for inherent micro porosity analysis using µCT. The results are included in Table 6 which shows that the mean size of inherent micro pores is almost the same for all thin walls (approximately equal to 20 µm) and is independent of process parameters. As stated before, these micro pores are produced by melting and have spherical shapes. As it was observed by SEM analysis, which will be presented later, inherent micro pores have diameters in the range of 2–50 µm. However, pores with diameters below

Table 4
CT scanning parameters.

Voltage	170 kV
Current	59 µA
Exposure time	2000 ms
Nr. of projections	1500
Filter	0.25 mm, copper
Voxel size	(6 µm)3

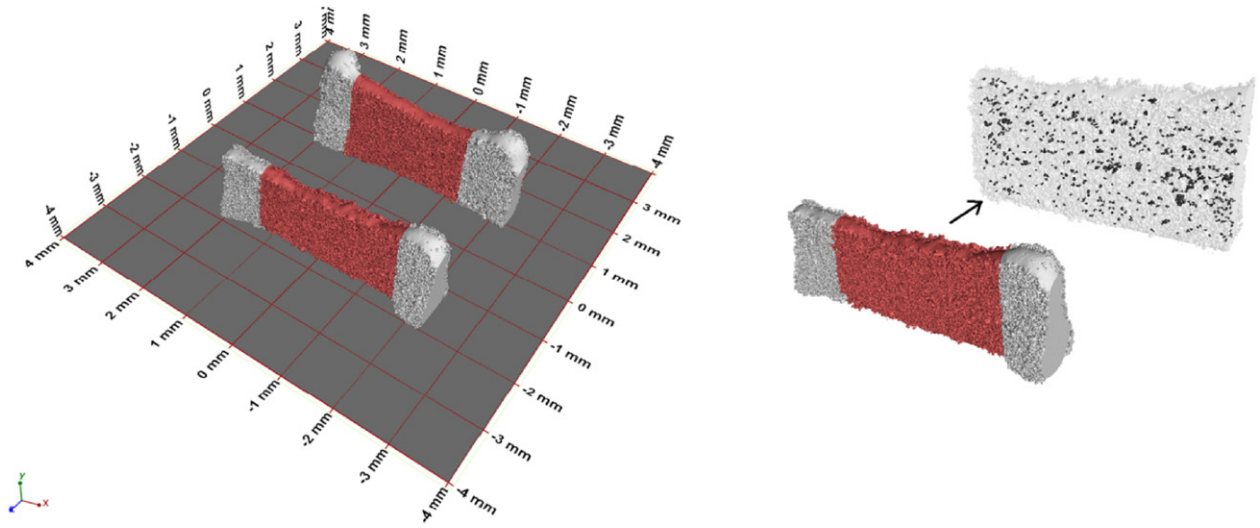

Fig. 4. μCT analysis of thin walls produced by μDMD and inherent micro pore analysis at the central part (red shaded areas).

Table 5
Scanning strategies used to produce NiTi cubes.

Strategy	Track's angle (θ_T)	Layer's angle (θ_L)	1st layer	2nd layer	3rd layer	4th layer
Strategy A	0	0				
Strategy B	0	90				
Strategy C	0	180				
Strategy D	180	0				
Strategy E	180	90				

$P = 25$ W, V = 150 mm/min, $d_H = 100$ μm, T = 200 °C, RF_n: 0.76 mg/s.

12 μm (i.e. volumes below about 8 voxels) were not considered in the μCT analysis, as they were considered too near the μCT resolution limit and hence they could be influenced by the noise of μCT data. Inserting the overlap between the layers at constant temperature decreases the inherent micro porosity percentage. The distribution of inherent micro pores in thin walls with 30% overlap between the layers is likely to be more homogenous in comparison with the walls without interlayer overlap, as it is shown for example in Fig. 8(a) and (b). From Fig. 9(a), it was concluded that heating the substrate up to 300 °C can reduce the inherent micro porosity percentage in NiTi thin walls. However, increasing the temperature of substrate up to 400 °C caused to increase in porosity percentage. This phenomenon can be explained by evaporation of NiTi because of high temperature of melt pool. This high temperature comes from the accumulation of input energy of μDMD process and temperature of substrate. Same trend also exists for the walls with 30% overlap between the layers (Fig. 9(b)).

According to Fig. 10, remelting the previous layer in the wall with overlap can reduce the inherent micro porosity in these walls. In fact, the effect of temperature in μDMD is twofold. Because of small laser focal spot in μDMD, input energy and consequently melt pool

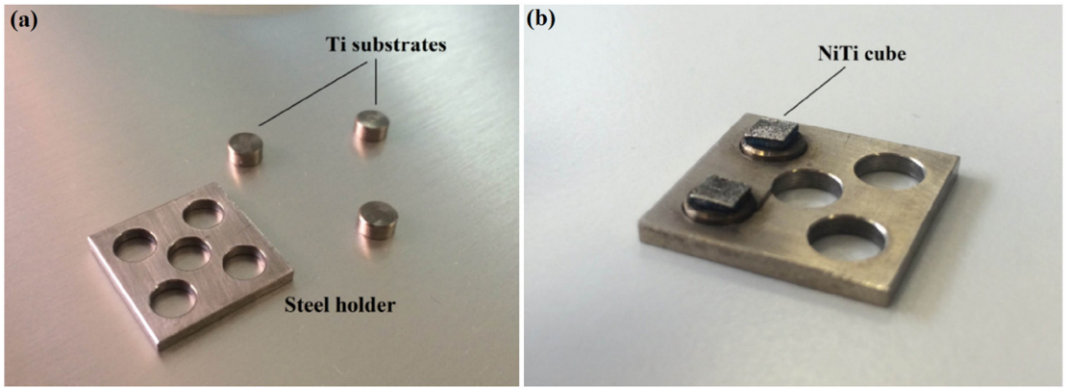

Fig. 5. (a): Steel 316 L holder and Ti pellet substrates, (b) NiTi cubes produced by μDMD.

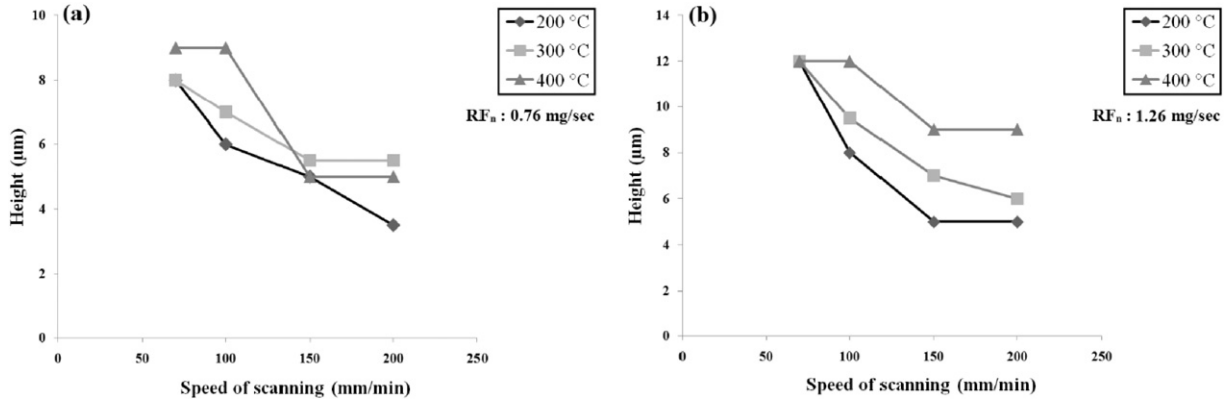

Fig. 6. Effect of scanning speed and substrate temperature on the height of single tracks produced by µDMD with (a) 0.76 mg/s and (b) 1.26 mg/s powder feeding rates.

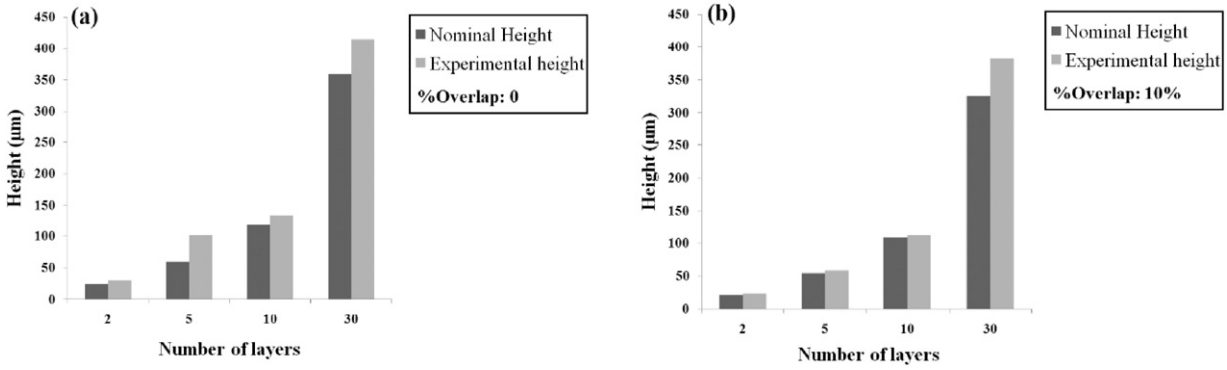

Fig. 7. Effect of layer overlap in fabrication of NiTi thin walls by µDMD.

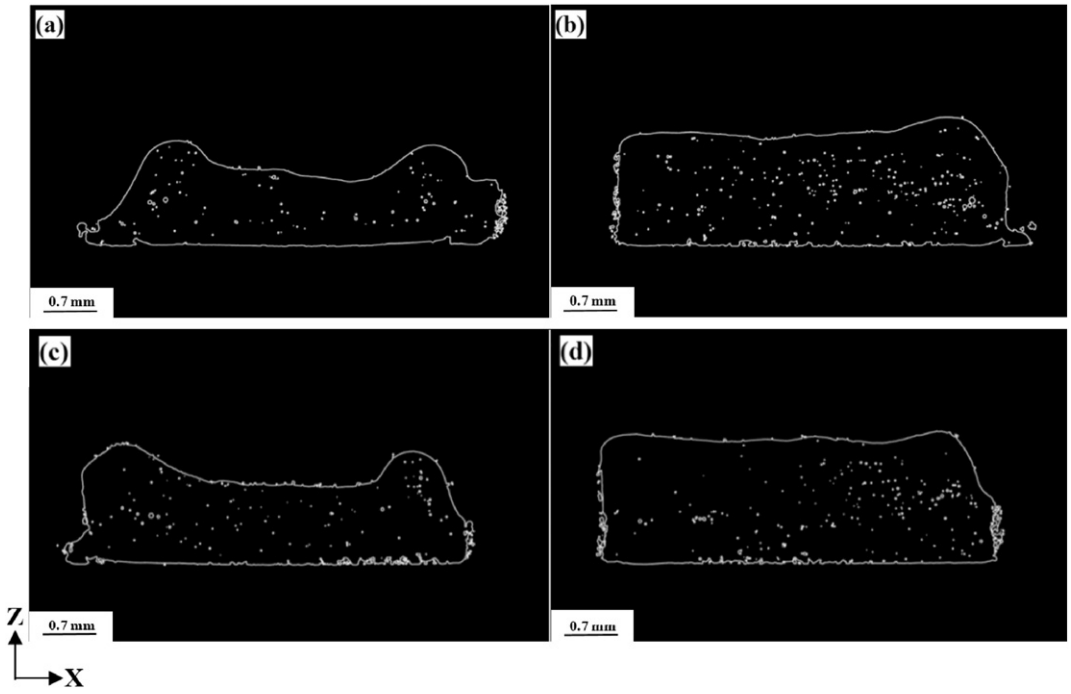

Fig. 8. Effect of layer overlap and temperature of substrate on shape and inherent micro porosity distribution of thin walls (a): T = 200 °C, V = 150 mm/min, %OV = 0%, porosity = 1.49%, (b): T = 200 °C, V = 150 mm/min, %OV = 30%, porosity = 0.98%, (c): T = 300 °C, V = 70 mm/min, %OV = 0%, porosity = 1.01%, (d): T = 300 °C, V = 70 mm/min, %OV = 30%, porosity = 0.79%.

Table 6
Inherent micro porosity analysis of NiTi thin walls using μCT scanning.

Wall	V (mm/min)	T (°C)	OV%	d_{IMP} (μm)	Porosity (%)	Mean height (mm)
1	70	200	0	19.64	0.84	0.9
2	150	200	0	18.07	1.49	1.37
3	70	200	30	19.27	0.92	1.43
4	150	200	30	21.00	0.98	1.63
5	70	300	0	20.34	0.72	1.13
6	150	300	0	20.34	1.01	1.11
7	70	300	30	20.34	0.72	1.61
8	150	300	30	20.00	0.79	1.46
9	70	400	0	18.07	1.29	1.14
10	150	400	0	17.63	1.37	0.78
11	70	400	30	18.49	0.96	1.47
12	150	400	30	19.27	0.85	1.13

P: 30 W, NH: 1 mm, d_{IMP}: mean diameter of inherent micro pores, OV%: overlap.

temperature are so high. Moreover, overlap between the layers increases the input energy produced by μDMD process and consequently increases the melt pool temperature. Generally, high temperature in laser melting process results in high density product formation that was reported by others [17]. But, using elevated temperature for substrate and overlap between the layers at the same time in μDMD encourages evaporation in the melt pool and increases the porosity (see Fig. 10).

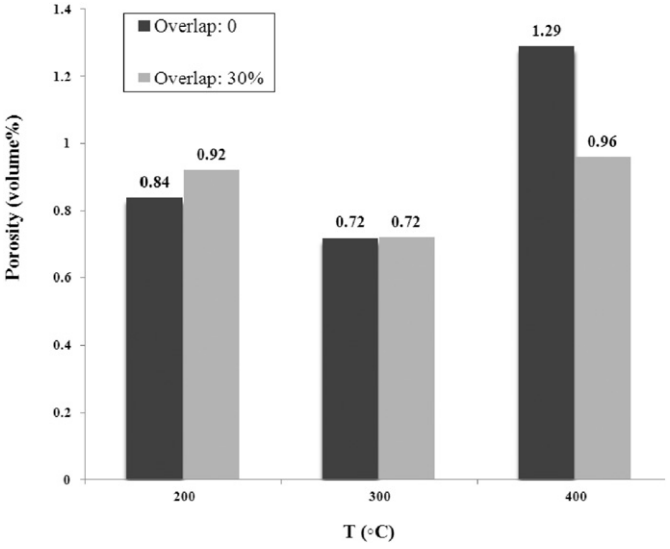

Fig. 10. Effect of layer overlap and temperature of substrate on inherent micro porosity of NiTi thin walls produced by μDMD.

3.2. The effect of μDMD process parameters on controllable micro porosity

As presented in the previous section, melting can produce inherent micro pores with spherical shape and about 20 μm mean pore sizes. It is not easy to manipulate the size, morphology and distribution of inherent micro pores. But, controllable micro pores are possible to fabricate using specific process parameters and CAD models [18]. Hatch distance and strategy of scanning are two important parameters in μDMD and their effects on micro porosity of NiTi cubes is discussed in this section. Strategy of scanning can affect the surface quality and pore characteristics of the parts produced by μDMD. To evaluate the effect of hatch distances on micro porosity formation in laser melted products, 3 cubes were fabricated by 3 different hatch distances. As shown in Fig. 11(a), when the hatch distances are small, there are overlaps between the single tracks and consequently the micro pores are small and the distribution of pores is not homogenous. Increase in hatch distances decreases the overlap between the tracks. This makes the morphology of pores more regular. Fig. 11(a) shows that near fully dense structure has been formed using 100 μm hatch distance. For further investigation, five NiTi cubes with different scanning strategies were fabricated according to Table 5 using 100 μm hatch distances.

Fig. 12 shows the scanning electron micrographs after polishing of NiTi cubes produced by different strategies of scanning according to Table 5. As it can be seen in Fig. 12, when a 90° rotation is applied between the layers (strategy B and E), the distribution of micro pores is more homogeneous and the pores are smaller and more rounded in comparison with the other strategies. Quantitative micro pore analysis of NiTi cubes produced by different scanning strategies is presented in Fig. 13, which shows that different strategies of scanning produce different porosity percentages and different pore sizes. Also, the trends of both graphs related to porosity percentages and micro pore sizes are the same. It is noteworthy that in the data presented in Fig. 13, both inherent and controllable micro porosity have been considered. So, it can

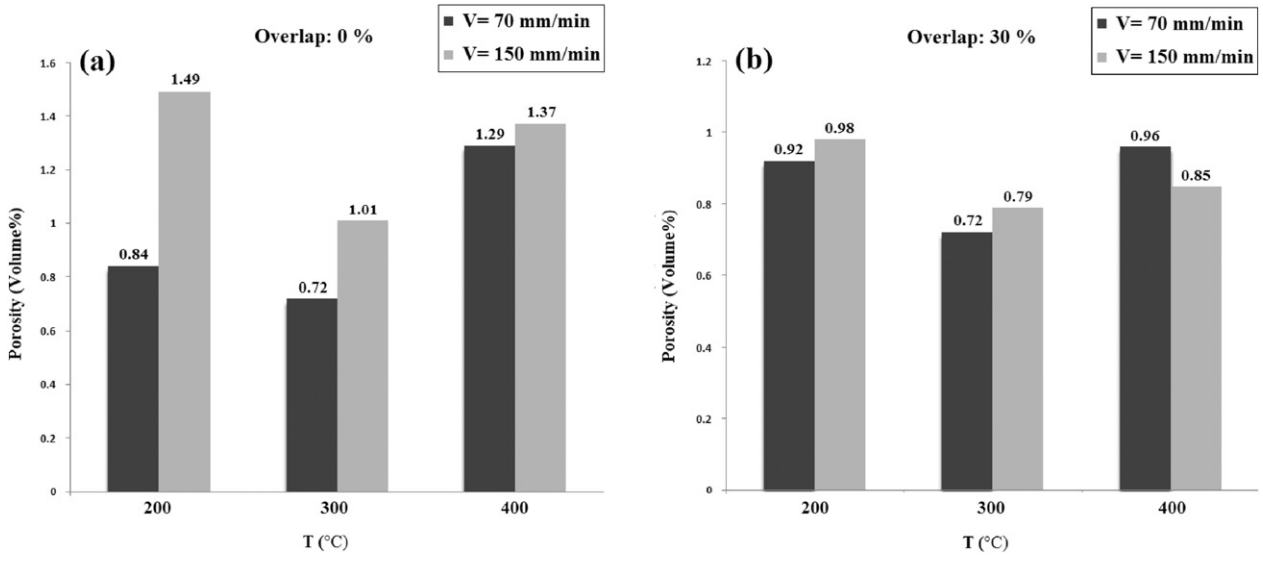

Fig. 9. Effect of scanning speed and temperature of substrate on inherent micro porosity of NiTi thin walls produced by μDMD (a): without overlap between the layers, (b): with 30% overlap between layers.

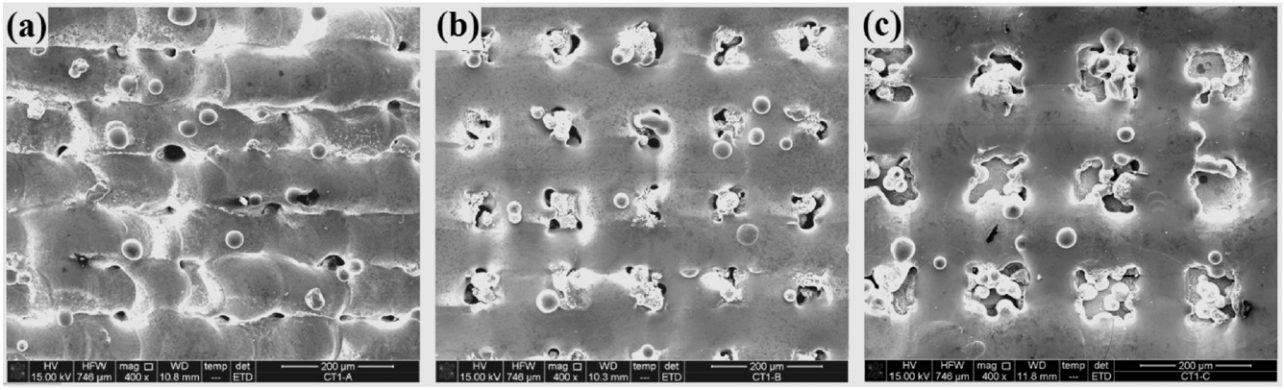

Fig. 11. SEM micrographs of top surface of NiTi cubes produced by μDMD with (a) 100 μm, (b) 150 μm, (c) 200 μm hatch distances. (T = 200 °C, *P* = 30 W, V = 100 mm/min, ΔZ = 4 μm, RF_n: 1.26 mg/s, strategy of scanning: strategy B according to Table 5).

be concluded that, using the same μDMD process parameters and different scanning strategies it is possible to manipulate the micro pore's size and morphology, which can be used to produce porous scaffolds with specific porous structures.

As stated before, bone ingrowth is not only dependent from pore size and porosity percentage but also from pore shape. Using image analysis method, it's possible to define pore's shape distribution in 2D images taken by SEM. P_C is the percentage of pores with specific range of circularity values (C) and can be written as:

$$P_C = (N_C / N_t) \times 100\% \quad (4)$$

where, N_C is the number of micro pores with defined range of circularity and N_t is the total number of micro pores in selected 2D area. A circularity value of 1.0 indicates a perfect circle. As the value approaches 0.0, it indicates an increasingly elongated polygon. As shown in Table 7, the maximum number of rounded micro pores (circularity: 0.6–1) is related to strategy E that confirms the previous findings.

Surface roughness of NiTi cubes produced by different scanning strategies was measured using 3D optical micrographs that are presented in Table 8. Table 8 shows that despite of lateral irregularity of NiTi cubes which have 90° rotation between successive layers (strategy B and E), the surface roughness of these two strategies are lower than the other strategies. In other words, the quality of surface is better when the angle between tracks and layers are 0 and 90 respectively. Also, using strategies B and E, results in minimum porosity percentage and minimum average pore size as presented before in Fig. 13.

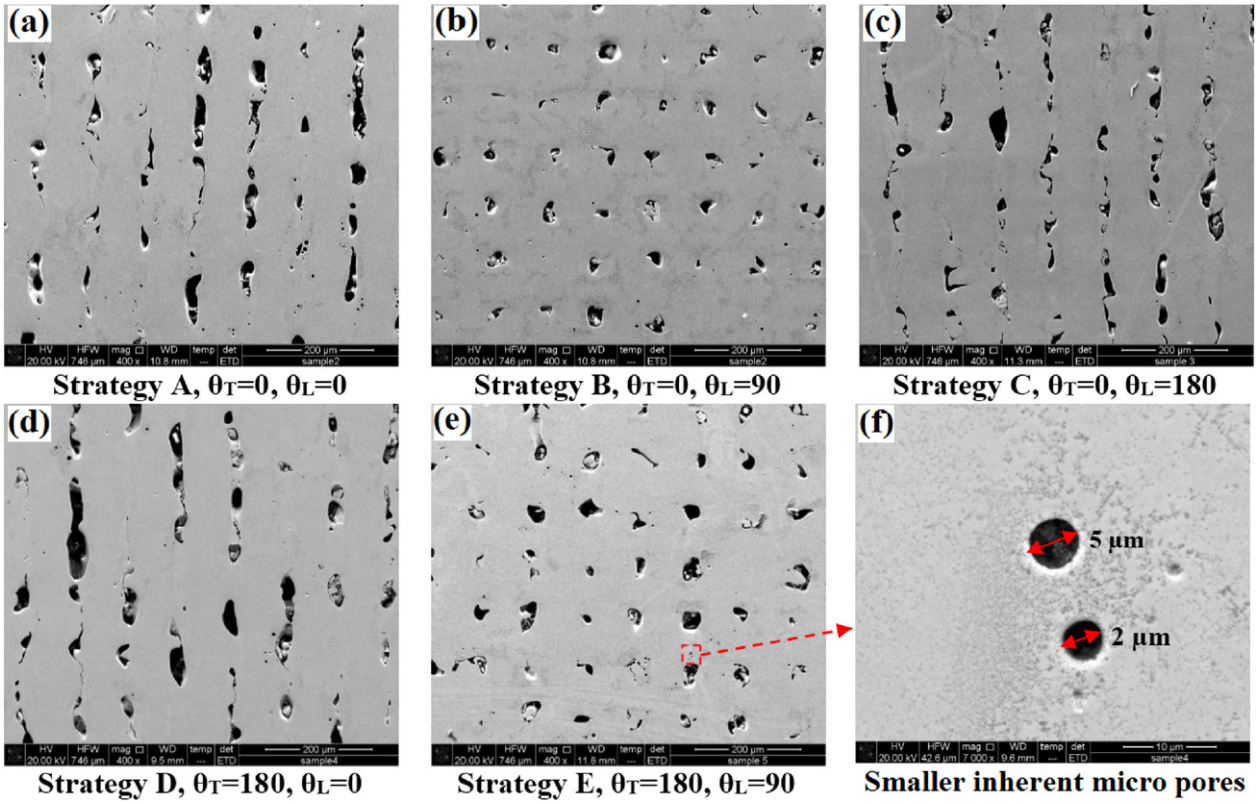

Fig. 12. SEM micrographs were taken of top surface of NiTi cubes produced by (a) strategy A, (b) strategy B, (c) strategy C, (d) strategy (D), (e) strategy E of scanning according to Table 5, (f) small inherent micro pores in higher magnification.

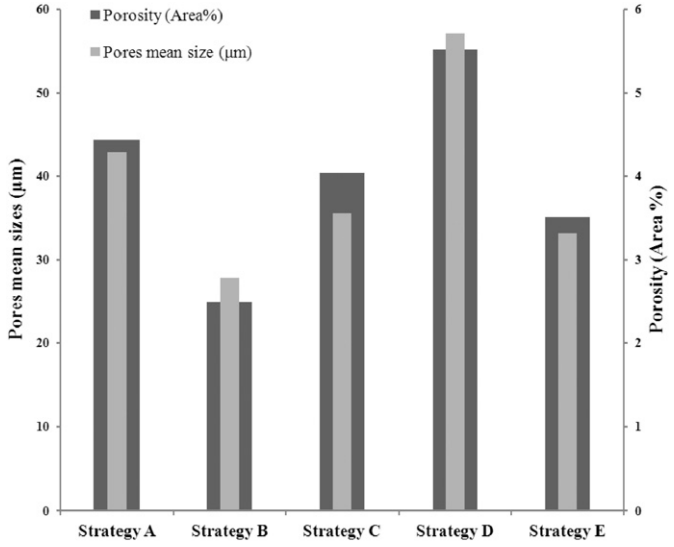

Fig. 13. Total porosity percentages and mean value of micro pore's sizes in laser melted NiTi cubes produced by different strategies of scanning.

Table 7
Micro pore's shape analysis of NiTi cubes produced by different scanning strategies according to Table 5.

Strategy	$P_{C:\ 0–0.3}$	$P_{C:\ 0.3–0.6}$	$P_{C:\ 0.6–1}$
Strategy A	55	47	18
Strategy B	53	50	18
Strategy C	56	46	14
Strategy D	54	45	12
Strategy E	44	40	27

Table 8
Surface quality of NiTi cubes.

Strategy	Track's angle	Layer's angle	Ra (μm)	Total porosity (%)
Strategy A	0	0	61.45	4.43%
Strategy B	0	90	39.28	2.50%
Strategy C	0	180	65.71	4.04%
Strategy D	180	0	103.96	5.52%
Strategy E	180	90	52.46	3.51%

4. Conclusions

The effects of micro direct metal deposition process parameters on evolution of inherent and controllable micro porosities in NiTi parts were analysed by means of scanning electron microscopy (SEM) and micro X-ray computed tomography (μCT) and discussed in this research. Main achievements of this work are summarized in the following points:

1. Raise in substrate's temperature generally facilitates the formation of 3D parts by μDMD. However, because of high level of input energy in μDMD process, there is an optimum temperature to achieve 3D part with minimum inherent micro porosity. This temperature is 300 °C for NiTi.
2. Overlap between the successive layers in parts produced by μDMD produces more accurate geometries and homogenous distribution of inherent micro pores.
3. Using different scanning strategies in μDMD process revealed that, when there is a 90° rotation between the scanning directions in subsequent layers, the distribution of controllable micro pores is more homogeneous and the pores are smaller and more rounded in comparison with the other strategies.

References

[1] A.P. Rubshtein, I.S. Trakhtenberg, E.B. Makarova, E.B. Triphonova, D.G. Bliznets, L.I. Yakovenkova, et al., Porous material based on spongy titanium granules: structure, mechanical properties, and osseointegration, Mater. Sci. Eng. C 35 (2014) 363–369.
[2] S. Bose, M. Roy, A. Bandyopadhyay, Recent advances in bone tissue engineering scaffolds, Trends Biotechnol. 30 (2012) 546–554.
[3] G. Ryan, A. Pandit, D.P. Apatsidis, Fabrication methods of porous metals for use in orthopaedic applications, Biomaterials 27 (2006) 2651–2670.
[4] T.B. Sercombe, X. Xu, V.J. Challis, R. Green, S. Yue, Z. Zhang, et al., Failure modes in high strength and stiffness to weight scaffolds produced by selective laser melting, Mater. Des. 67 (2015) 501–508.
[5] Y.J. Liu, X.P. Li, L.C. Zhang, T.B. Sercombe, Processing and properties of topologically optimised biomedical Ti–24Nb–4Zr–8Sn scaffolds manufactured by selective laser melting, Mater. Sci. Eng. A 642 (2015) 268–278.
[6] B.V. Krishna, S. Bose, A. Bandyopadhyay, Fabrication of porous NiTi shape memory alloy structures using laser engineered net shaping, J. Biomed. Mater. Res. B Appl. Biomater. 89 (2009) 481–490.
[7] M.N. Ahsan, C.P. Paul, L. Kukreja, A.J. Pinkerton, Porous structures fabrication by continuous and pulsed laser metal deposition for biomedical applications; modelling and experimental investigation, J. Mater. Process. Technol. 211 (2011) 602–609.
[8] S. Khademzadeh, N. Parvin, P.F. Bariani, Production of NiTi alloy by direct metal deposition of mechanically alloyed powder mixtures, Int. J. Precis. Eng. Manuf. 16 (2015) 2333–2338.
[9] T.M.G. Chu, D.G. Orton, S.J. Hollister, S.E. Feinberg, J.W. Halloran, Mechanical and in vivo performance of hydroxyapatite implants with controlled architectures, Biomaterials 23 (2002) 1283–1293.
[10] A. Mikos, G. Sarakinos, M. Lyman, D. Ingber, J. Vacanti, R. Langer, Prevascularization of porous biodegradable polymers, Biotechnol. Bioeng. 42 (1993) 716–723.
[11] S.J. Simske, R.A. Ayers, T. Bateman, Porous materials for bone engineering, Mater. Sci. Forum 250 (1997) 151–182.
[12] M. Balcon, S. Carmignato, E. Savio, Performance verification of a confocal microscope for 3D metrology tasks, Qual. — Access to Success 13 (2012) 63–66.
[13] S. Carmignato, D. Dreossi, L. Mancini, F. Marinello, G. Tromba, E. Savio, Testing of x-ray microtomography systems using a traceable geometrical standard, Meas. Sci. Technol. 20 (2009) 1–7.
[14] S. Carmignato, Accuracy of industrial computed tomography measurements: experimental results from an international comparison, CIRP Ann. Manuf. Technol. 61 (2012) 491–494.
[15] L. Peng, Y. Taiping, L. Sheng, L. Dongsheng, H. Qianwu, X. Weihao, Direct laser fabrication of nickel alloy samples, Int. J. Mach. Tools Manuf. 45 (2005) 1288–1294.
[16] I.V. Shishkovskii, I.A. Yadroitsev, I.Y. Smurov, Selective laser sintering/melting of nitinol–hydroxyapatite composite for medical applications, Powder Metall. Met. Ceram. 50 (2011) 275–283.
[17] H. Meier, C. Haberland, Experimental studies on selective laser melting of metallic parts, Mater. Werkst. 39 (2008) 665–670.
[18] V. Karageorgiou, D. Kaplan, Porosity of 3D biomaterial scaffolds and osteogenesis, Biomaterials 26 (2005) 5474–5491.